Letter Vol. 50, No. 19/1 October 2025/Optics Letters 6077

Diversity-enhanced multicarrier transmission for secure, band-limited, and turbulent UOWC systems

Yang Ye,[1] Chen Chen,[1,*] Zhihong Zeng,[1] Dengke Wang,[1] and Harald Haas[2]

[1]School of Microelectronics and Communication Engineering, Chongqing University, Chongqing 400044, China
[2]Department of Engineering, University of Cambridge, 9 JJ Thomson Avenue, Cambridge CB3 0FA, United Kingdom
*c.chen@cqu.edu.cn

Received 15 June 2025; revised 22 August 2025; accepted 27 August 2025; posted 27 August 2025; published 23 September 2025

Low-pass band limitation and turbulence are two critical issues faced by practical underwater optical wireless communication (UOWC) systems. In this Letter, we propose an orthogonal frequency division multiplexing (OFDM)-based diversity-enhanced multicarrier (D-MC) scheme for joint mitigation of low-pass band limitation and turbulence issues in UOWC systems. The OFDM-based D-MC scheme is realized by performing diversity transmission in both the frequency and time domains during OFDM modulation. Moreover, to enhance the security of OFDM-based D-MC transmission, a two-stage chaotic encryption scheme is further proposed which includes chaotic phase rotation and chaotic scrambling. Experimental results show that OFDM-based D-MC with 2D diversity can achieve a substantial 69.9% usable bandwidth extension compared with the conventional scheme without diversity.

https://doi.org/10.1364/OL.570771

With the growing demand for underwater activities ranging from ocean exploration to marine environmental monitoring, the development of high-speed underwater wireless communication technologies has become increasingly important for practical applications. In recent years, underwater optical wireless communication (UOWC) has been envisioned as a potential candidate to establish high-speed wireless connectivity in the underwater environments, owing to its advantages of large bandwidth, high data rate, low propagation latency, high security, small size, and low power consumption [1]. Nevertheless, practical UOWC systems usually suffer from two critical challenges: low-pass band limitation introduced by the adopted commercial light sources, such as light-emitting diodes (LEDs) and laser diodes (LDs), and underwater turbulence induced by the sudden variations in water temperature and pressure because of ocean currents or air bubbles [2]. Low-pass band limitation will limit the usable bandwidth of the UOWC system as the high-frequency components of the transmitted signal might experience relatively severe power attenuation, while underwater turbulence will lead to significant amplitude fluctuation of the received signal. Hence, the overall performance of practical UOWC systems might be greatly degraded by the low-pass band limitation and underwater turbulence issues.

So far, various techniques have been proposed to address the low-pass band limitation issue in UOWC systems such as pre-equalization [3], pre-emphasis [4], and non-orthogonal multiple access (NOMA) [5]. Nevertheless, channel feedback information is generally required to employ these techniques. Moreover, diversity transmission schemes have also been proposed to enhance the performance of UOWC systems by mitigating the low-pass and turbulence effects. For the low-pass band limitation issue, a spectrum spread orthogonal frequency division multiplexing (OFDM) scheme was proposed in [6], where multiple subcarriers were employed to transmit the same data symbol. Therefore, this frequency diversity transmission scheme can result in improved signal-to-noise ratio (SNR) performance at the receiver side. Moreover, an orthogonal frequency division diversity and multiplexing (OFDDM) scheme was further proposed in [7], where the subcarriers were divided into subblocks with subblock interleaving, and each subblock was used to transmit the same data symbol. The OFDDM scheme can achieve a flexible trade-off between diversity and multiplexing during multicarrier transmission. For the underwater turbulence issue, time diversity transmission schemes can be generally considered to efficiently mitigate the turbulence-induced signal fading [8–10]. Besides time diversity transmission, several spatial diversity transmission schemes have also been reported such as multiple-input single-output transmission [11], single-input multiple-output transmission [12], multiple-input multiple-output transmission [13], and spatial division transmission [14]. However, spatial diversity transmission is realized via introducing more optical transmitters and/or receivers, which inevitably increases the overall complexity and cost of the UOWC system. To the best of our knowledge, the joint mitigation of both low-pass band limitation and underwater turbulence issues in UOWC systems has not yet been reported in the literature.

Aiming at jointly mitigating low-pass band limitation and underwater turbulence, we propose and experimentally demonstrate an OFDM-based diversity-enhanced multicarrier (D-MC) scheme for UOWC systems, which is realized by performing diversity transmission in both the frequency and time domains during OFDM modulation. Based on the proposed OFDM-based D-MC scheme, a two-stage chaotic encryption scheme is further designed to enhance the transmission security of UOWC systems. Hardware experiments are conducted to investigate and compare the performance of the proposed OFDM-based D-MC scheme with two-stage chaotic encryption with other benchmark

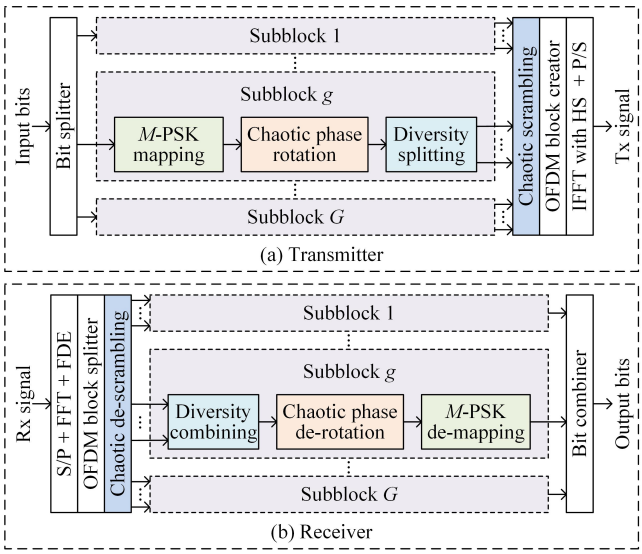

Fig. 1. Schematic diagram of OFDM-based D-MC with two-stage chaotic encryption: (a) transmitter and (b) receiver.

schemes in an experimental UOWC system with low-pass band limitation and bubble turbulence.

Figure 1 depicts the schematic diagram of OFDM-based D-MC with two-stage chaotic encryption. At the transmitter, as shown in Fig. 1(a), the input bits are first split into G streams via a bit splitter and each bit stream is then sent into a subblock with length n, where $n = N/G$ with N being the number of data subcarriers in OFDM modulation. In each subblock, M-ary phase shift keying (M-PSK) mapping is first performed to convert the information bits into M-PSK symbols. After that, the first-stage chaotic encryption, i.e., chaotic phase rotation, is conducted to encrypt the phase of the generated M-PSK symbols. Subsequently, diversity splitting is executed in the frequency domain (FD) and/or time domain (TD) in each subblock. By defining d as the diversity factor, a total of d subcarriers in the FD and/or TD are utilized to simultaneously transmit the same M-PSK symbol so as to harvest diversity gain at the receiver side. Before OFDM block creation, the second-stage chaotic encryption, i.e., chaotic scrambling, is further carried out to scramble the positions of the M-PSK symbols in the input symbol vector. Finally, the transmitted signal can be obtained via inverse fast Fourier transform (IFFT) with Hermitian symmetry (HS) and parallel-to-serial (P/S) conversion. At the receiver, as shown in Fig. 1(b), the received signal first undergoes serial-to-parallel (S/P) conversion, fast Fourier transform (FFT), frequency domain equalization (FDE) and OFDM block splitting. After that, chaotic de-scrambling is done to recover the transmitted M-PSK symbol vectors. To recover the information bits in each subblock, maximum ratio combining (MRC)-based diversity combining [15], chaotic phase de-rotation and M-PSK de-mapping are sequentially performed, and the final output bits are generated via combining the recovered bits of all the subblocks.

The principle of the D-MC scheme with various diversity transmission approaches is illustrated in Fig. 2, where the subblock length is assumed to be $n = 2$ and a total of two consecutive time slots is considered here. Let d denote the diversity factor, i.e., the number of subcarriers to transmit the same M-PSK symbol in each subblock. For the case without diversity (i.e., $d = 1$), as shown in Fig. 2(a), all the four subcarriers in

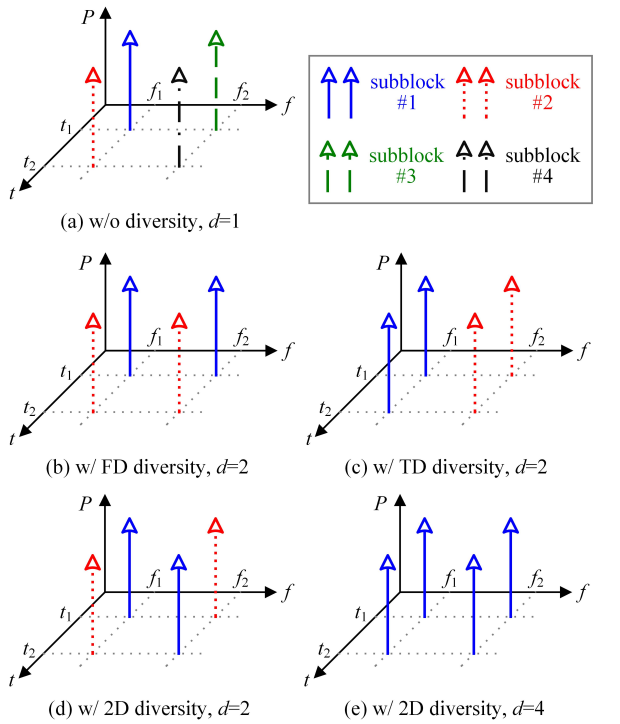

Fig. 2. Principle of the D-MC scheme: (a) without diversity, $d = 1$, (b) with FD diversity, $d = 2$, (c) with TD diversity, $d = 2$, (d) with 2D diversity, $d = 2$, and (e) with 2D diversity, $d = 4$.

the subblock over two time slots are employed to transmit four different M-PSK symbols. For FD diversity with $d = 2$, as shown in Fig. 2(b), the two subcarriers at the same time slot over two frequencies are used to transmit the same M-PSK symbol. Similarly, for TD diversity with $d = 2$, as shown in Fig. 2(c), the two subcarriers at the same frequency over two time slots are used to transmit the same M-PSK symbol. For both 1D diversity schemes including FD diversity and TD diversity, a total of two M-PSK symbols can be transmitted by the subblock over two time slots. In order to jointly mitigate FD low-pass effect and TD turbulence, two 2D diversity schemes are proposed. For 2D diversity with $d = 2$, as can be seen from Fig. 2(d), the subcarrier at frequency f_1 and time slot t_1 is paired together with the subcarrier at frequency f_2 and time slot t_2 to transmit the same M-PSK symbol, while the remaining two subcarriers are also paired to transmit another M-PSK symbol. Moreover, for 2D diversity with $d = 4$, as can be seen from Fig. 2(d), all the four subcarriers in the subblock over two time slots are utilized to transmit the same M-PSK symbol. As shown in Fig. 2, compared with the case without diversity (i.e., $d = 1$) using the M-PSK constellation, the diversity transmission approach with a diversity factor d needs to use a M^d-PSK constellation to achieve the same data rate.

To enhance the security of OFDM-based D-MC transmission, a two-stage chaotic encryption scheme is further designed. The first-stage chaotic encryption is chaotic phase rotation, which is conducted to encrypt the phase of the generated M-PSK symbols. Taking quadrature PSK (QPSK) as an example, as shown in Figs. 3(a) and 3(b), the k-th QPSK symbol after chaotic phase rotation in the g-th subblock is given by

$$s_k^g = A\exp(\phi_k^g + p_k^g), \tag{1}$$

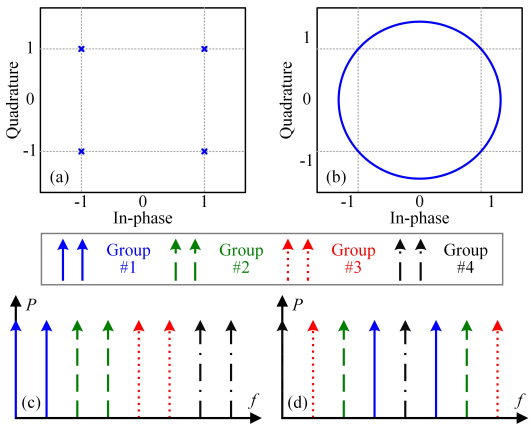

Fig. 3. Illustration of QPSK constellation: (a) without and (b) with chaotic phase rotation, and subcarrier grouping: (c) without and (d) with chaotic scrambling.

where we have $s_k^g \in \mathbf{s}^g$ with $\mathbf{s}^g$ being the QPSK symbol vector with length K and $k = 1, 2, \cdots, K$, A is the amplitude, $\phi_k^g \in \{-\pi/4, \pi/4, 3\pi/4, 5\pi/4\}$ is the initial phase and p_k^g is the additional phase rotation added to encrypt the QPSK symbol. Specifically, the chaotic phase rotation vector $\mathbf{p}^g$ for the g-th subblock can be generated as follows:

$$\mathbf{p}^g = src\{\mathbf{q}, \mathbf{a}^g\}, \tag{2}$$

where $src\{\cdot,\cdot\}$ is the scrambling function, $\mathbf{q} = [q_1, q_2, \cdots, q_K]^T$ is a uniformly distributed phase vector between 0 and 2π with length K, and $\mathbf{a}^g$ is the corresponding permutation vector. The scrambling function scrambles $\mathbf{q}$ according to $\mathbf{a}^g$ which indicates the new positions of the elements in $\mathbf{p}^g$.

Moreover, the second-stage chaotic encryption is chaotic scrambling, which is carried out to scramble the positions of the M-PSK symbols in the input symbol vector before OFDM block creation. Letting $\mathbf{x}^k = [x_1^k, x_2^k, \cdots, x_N^k]^T$ denote the input symbol vector at the k-th time instant, the resultant symbol vector $\mathbf{y}^k$ after chaotic scrambling is given by

$$\mathbf{y}^k = src\{\mathbf{x}^k, \mathbf{b}^k\}, \tag{3}$$

where $\mathbf{b}^k$ is the permutation vector to perform chaotic scrambling which indicates the new positions of the elements in $\mathbf{y}^k$.

In order to successfully perform the two-stage chaotic encryption scheme in the OFDM-based D-MC transmission, the permutation vectors $\mathbf{a}^g$ and $\mathbf{b}^k$ should be determined first. In this work, the 2D Logistic map is adopted as the chaotic map to realize chaotic encryption [16], which is defined as follows:

$$\begin{cases} x_{t+1} = \alpha_1 x_t (1 - x_t) + \beta_1 y_t^2 \\ y_{t+1} = \alpha_2 y_t (1 - y_t) + \beta_2 (x_t^2 + x_t y_t) \end{cases}, \tag{4}$$

where t is the discrete time index, $0 < x_t \le 1$ and $0 < y_t \le 1$. It has been shown that the system defined by Eq. (4) falls into the chaotic domain when $2.75 < \alpha_1 \le 3.4$, $2.75 < \alpha_2 \le 3.45$, $0.15 < \beta_1 \le 0.21$, and $0.13 < \beta_2 \le 0.15$. It has been verified in [17] that the sequences x_t and y_t generated by such a system have high unpredictability, randomness and sensitivity to the initial values.

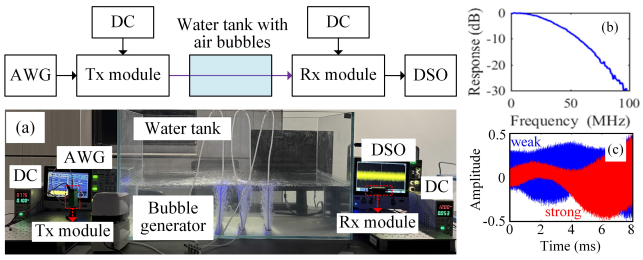

Fig. 4. Experimental setup of the UOWC system. Insets: (a) testbed photo, (b) system response, and (c) received waveforms.

Based on the chaotic system given by Eq. (4), the permutation vectors $\mathbf{a}^g$ and $\mathbf{b}^k$ can be respectively generated by the states x_t and y_t as follows:

$$\begin{cases} \mathbf{a}^g = sort\{x_{(g-1)K+1}, x_{(g-1)K+2}, \cdots, x_{gK}\} \\ \mathbf{b}^k = sort\{y_{(k-1)N+1}, x_{(k-1)N+2}, \cdots, x_{kN}\} \end{cases}, \tag{5}$$

where $sort\{\cdot\}$ denotes the sorting function which returns the index vector of the elements of the input vector by sorting these elements in a descending order. In the chaotic system given by Eq. (4), the initial values x_0, y_0 and the parameters α_1, α_2, β_1, β_2 can be set as the security keys. According to the IEEE standard for binary floating-point arithmetic [16], the computational precision of a 64-bit double-precision number is approximately 10^{-15}. Considering $0 < x_0 \le 1$, $0 < y_0 \le 1$, $2.75 < \alpha_1 \le 3.4$, $2.75 < \alpha_2 \le 3.45$, $0.15 < \beta_1 \le 0.21$, and $0.13 < \beta_2 \le 0.15$, the key space of the two-stage chaotic encryption can be calculated by $10^{15} \times 10^{15} \times 0.65 \times 10^{15} \times 0.7 \times 10^{15} \times 0.06 \times 10^{15} \times 0.02 \times 10^{15} = 5.46 \times 10^{86}$.

To evaluate the performance of the proposed OFDM-based D-MC scheme and compare it with other benchmark schemes in band-limited and turbulent UOWC systems, we conduct hardware experiments in a lab environment. The experimental setup of the turbulent UOWC system is depicted in Fig. 4, where the transmitted signal is first generated offline by MATLAB and then loaded to an arbitrary waveform generator (AWG, Tektronix AFG31102) with a sampling rate of 250 MSa/s. The AWG output signal with a peak-to-peak voltage of 250 mV is used to drive a commercial off-the-shelf optical transmitter module (HCCLS2021MOD01-Tx), which is powered by a DC bias of 12 V. A 1-m water tank filled with tap water is adopted to emulate the water channel and an air pump with multiple bubble strips is used together to generate the bubble turbulence. After propagating through the turbulent water channel, an optical receiver module (HCCLS2021MOD01-Rx) is adopted to receive the light signal which is also powered by a 12-V DC bias voltage. For more details about the adopted optical transmitter and receiver modules, please refer to our previous work [18]. The detected signal is recorded by a digital storage oscilloscope (DSO, Tektronix MDO32) with a sampling rate of 1.25 GSa/s and the obtained data are further processed offline using MATLAB. In OFDM modulation/demodulation, the IFFT/FFT size is set to 256, and the effective bandwidth of the OFDM signal is adjusted by varying the number of data subcarriers. The insets (a), (b), and (c) in Fig. 4 show the photo of the testbed, the system response, and the received waveforms, respectively. It can be observed that the experimental UOWC system exhibits a notable low-pass frequency response and the received waveforms experience significant amplitude fluctuations.

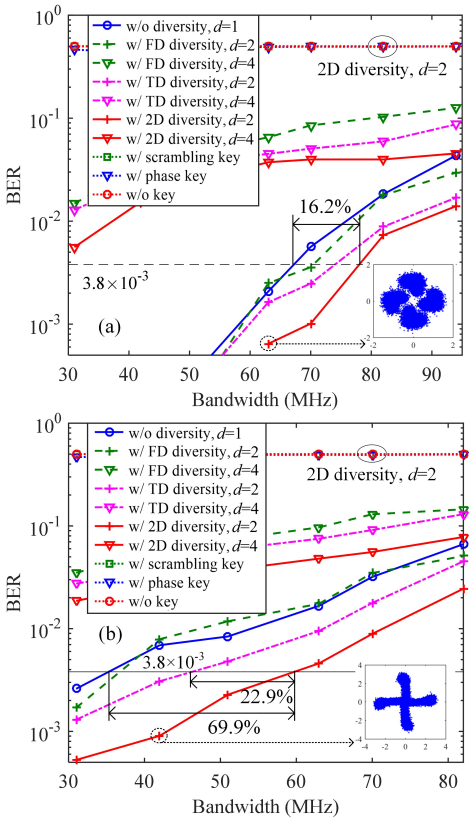

Fig. 5. Measured BER versus bandwidth for different schemes under (a) weak turbulence and (b) strong turbulence.

Figure 5 shows the bit error rate (BER) performance versus the effective bandwidth of the OFDM signal using different D-MC schemes under weak and strong turbulence conditions. The target spectral efficiency (SE) of all the schemes is assumed to be 1 bit/s/Hz, and hence the adopted PSK constellation orders for d = 1, 2, and 4 are M = 2, 4, and 16, respectively. We first assume that successful two-stage chaotic decryption can be realized at the receiver side by utilizing the shared security keys. For the case of weak turbulence where three bubble strips are used, as shown in Fig. 5(a), FD diversity with $d=2$ can only slightly outperform the conventional scheme without diversity, while TD diversity with $d=2$ performs better than FD diversity with $d=2$. Evidently, 2D diversity with $d=2$ performs the best which can achieve a usable bandwidth of 78 MHz at the 7% forward error correction (FEC) coding threshold of BER = 3.8×10^{-3}, which is corresponding to a 16.2% bandwidth extension in comparison to the conventional scheme without diversity. For the case of strong turbulence where four bubble strips are used, as can be seen from Fig. 5(b), 2D diversity with $d=2$ reaches the largest usable bandwidth of 59.8 MHz and the bandwidth extension is substantially increased to 69.9% when compared with the conventional scheme without diversity. Moreover, a remarkable 22.9% bandwidth extension can also be obtained by 2D diversity with $d=2$ in comparison to TD diversity with $d=2$. The insets in Figs. 5(a) and 5(b) show the corresponding received constellation diagrams.

It can also be observed from Figs. 5(a) and 5(b) that all the diversity schemes with $d=4$ cannot reach the 7% FEC coding threshold of BER = 3.8×10^{-3} under both weak and strong turbulence conditions. This is mainly due to the fact that a relatively large PSK constellation order of 16 is adopted for these schemes to achieve the target SE of 1 bit/s/Hz, which requires a much higher received SNR to achieve satisfactory BER performance. Moreover, we assume that the two-stage chaotic decryption cannot be successfully realized at the receiver side due to the lack of total or partial security keys for the eavesdropper. As we can see, for both weak and strong turbulence conditions, the resultant BERs without scrambling key, without phase key, and without both scrambling and phase keys are all around 0.5, indicating the feasibility of two-stage chaotic decryption to ensure transmission security in band-limited and turbulent UOWC systems using the proposed OFDM-based D-MC scheme.

In this Letter, we have proposed and experimentally demonstrated an OFDM-based D-MC scheme with two-stage chaotic encryption for secure, band-limited, and turbulent UOWC systems. By performing diversity transmission in both the frequency and time domains during OFDM modulation, OFDM-based D-MC transmission can be realized to jointly address the adverse FD low-pass effect and TD underwater turbulence. Moreover, a two-stage chaotic encryption scheme including chaotic phase rotation and chaotic scrambling is further proposed to enhance the security of OFDM-based D-MC transmission. Experimental results successfully verify the feasibility and superiority of the proposed OFDM-based D-MC scheme with two-stage chaotic encryption over benchmark schemes. Although this work is conducted under lab conditions, the obtained results can be generalized to actual oceanic environments.

Funding. National Natural Science Foundation of China (62271091); Natural Science Foundation of Chongqing Municipality (cstc2021jcyj-msxmX0480).

Disclosures. The authors declare no conflicts of interest.

Data availability. Data underlying the results presented in this paper are not publicly available at this time but may be obtained from the authors upon reasonable request.

REFERENCES

1. Z. Zeng, S. Fu, H. Zhang, *et al.*, IEEE Commun. Surv. Tutorials **19**, 204 (2017).
2. J. Xu and Y. Zhang, J. Light. Technol. **43**, 1644 (2025).
3. C. Chen, Y. Nie, M. Liu, *et al.*, IEEE Photon. Technol. Lett. **33**, 1081 (2021).
4. G. Krishna, J. Mathew, and S. Gupta, Appl. Opt. **63**, 8857 (2024).
5. G. Krishna, J. Mathew, and S. Gupta, Opt. Commun. **555**, 130248 (2024).
6. J. Zhang, G. Gao, J. Zhang, *et al.*, Opt. Exp. **30**, 17140 (2022).
7. J. Chen, C. Chen, Z. Zeng, *et al.*, Photonics **11**, 1051 (2024).
8. E. J. Lee and V. W. Chan, IEEE J. Sel. Areas Commun. **22**, 1896 (2004).
9. F. Xu, A. Khalighi, P. Caussé, *et al.*, Opt. Exp. **17**, 872 (2009).
10. K. Balaji and K. Prabu, Opt. Commun. **410**, 643 (2018).
11. M. A. A. Ali, Opt. Quantum Electron. **52**, 1 (2020).
12. W. Liu, Z. Xu, and L. Yang, Photon. Res. **3**, 48 (2015).
13. M. V. Jamali, J. A. Salehi, and F. Akhoundi, IEEE Trans. Commun. **65**, 1176 (2017).
14. J. Wang, C. Chen, B. Deng, *et al.*, Opt. Exp. **31**, 16812 (2023).
15. C. Chen, W.-D. Zhong, H. Yang, *et al.*, J. Light. Technol. **36**, 3603 (2018).
16. Y. Yang, C. Chen, W. Zhang, *et al.*, Opt. Exp. **26**, 34031 (2018).
17. Q. Zhang, L. Guo, and X. Wei, Math. Comput Model **52**, 2028 (2010).
18. C. Chen, Y. Nie, X. Zhong, *et al.*, in *Asia Communications and Photonics Conference (ACP)* (2021), p. 1.